Observation of the transition from inverted coupled-resonator-induced transparency to inverted Autler-Townes splitting

Daiki Sugio,[1] Takahiro Manabe,[1] Keigo Nakamura,[1] Takahiro Matsumoto,[2] and Makoto Tomita[1]
[1]*Department of Physics, Faculty of Science, Shizuoka University, 836, Ohya, Suruga-ku, Shizuoka, 422-8529, Japan*
[2]*Graduate School of Design and Architecture, Nagoya City University, Nagoya, 464-0083, Japan*

(Received 4 September 2022; accepted 23 December 2022; published 20 January 2023)

Inverted coupled-resonator-induced transparency eliminates amplification as a result of destructive interference between two competing excitation pathways and induces a "nonamplifying" transparency window in an otherwise strongly amplifying spectral region. Using coupled ring resonators as a model system, we systematically examined the transition from inverted induced transparency to Autler-Townes splitting (ATS) by controlling the coupling strength between two resonators. The inverted induced transparency spectrum transitioned into different ATS spectra depending on the parameters of the resonators. We also examined the transition that occurs when the second resonator has gain. In this case, the system showed enhanced transparency, in which the intensity of the induced window was much greater than the incident laser level.

DOI: 10.1103/PhysRevA.107.013110

I. INTRODUCTION

The Fano effect is a ubiquitous phenomenon that occurs when one or more discrete levels interact with a continuum of states [1,2]. This effect has been observed for a wide variety of physical systems, including diffraction grating anomalies, neutron scattering, tunneling spectroscopy, and quantum dots in the Aharonov-Bohm interferometer.

Electromagnetically induced transparency (EIT) [3,4] and related phenomena [5–14] are manifestations of Fano interference. EIT is a result of destructive interference between two competing excitation pathways. This effect eliminates system absorption and produces a transparent spectral window in an otherwise strongly absorbing spectral region. Similar effects have been observed in a range of systems, including systems involving coupled-resonator-induced transparency (CRIT) of two ultrahigh Q microspheres [5–9] and plasmon and metamaterials [10–12], as well as optomechanical systems that utilize radiation-pressure coupling between an optical cavity and mechanical oscillator [13,14]. Applications of EIT and related phenomena have been discussed extensively [15–20].

Conventionally, induced transparency is studied in passive systems [3–14], i.e., systems that suffer absorption or intrinsic losses. When the system utilizes gain, the physics is more interesting [21–23]. In a previous paper [24], we demonstrated inverted CRIT in a gain system. Inverted CRIT eliminates amplification rather than absorption owing to the destructive interference between two competing excitation pathways, which produces a "nonamplifying" transparency window. This effect offers more flexibility for photonic designs. For example, unlike typical CRIT, anomalous dispersion occurs in inverted CRIT. The steep and controllable anomalous dispersion was used to generate a smooth pulse peak at the output port from a peak-truncated Gaussian-shaped temporal pulse [25]. A unique feature of this inverted CRIT peak is that the peak is not attenuated (or amplified); thus, its intensity is identical to that of the original input pulse before truncation. Discussions on inverted induced transparency and potential applications for controlling light propagation have developed in other fields, including optomechanical systems [26].

Autler-Townes splitting (ATS) is another phenomenon that reduces absorption [27–32]. Unlike EIT, the ATS mechanism is comparable to the ac-Stark effect. Absorption reduction is caused by a doublet structure in the atomic absorption profile driven by strong electromagnetic pumping. It is important to distinguish ATS from EIT, as EIT is crucial for many applications including optically controlled slowing of light and optical storage. Different types of three-level atomic systems were investigated and two main system categories were found, those that show EIT interference and those that do not [27]. A classical analogy to ATS is mode splitting owing to the strong coupling between resonances. EIT and ATS discrimination has been studied extensively using an objective method based on the Akaike information criterion [28] and a time-domain approach [30].

Our intention is to examine the transition from inverted induced transmission to ATS in gain systems. The EIT to ATS transitions studied to date were limited to passive systems with absorption or losses; this transition has not been observed in gain systems. Here, we are interested in how a single gain peak accompanied with an induced window dip develops in doublet structures. As the coupled resonator is the only system that has been used to successfully realize an inverted induced transparency window, we used the resonator as a model system, and examined the transition from inverted CRIT to ATS by controlling the coupling strength between two resonators. The inverted CRIT spectrum transitioned into different types of ATS spectra depending on the resonator parameters. We also examined the transition that occurs when

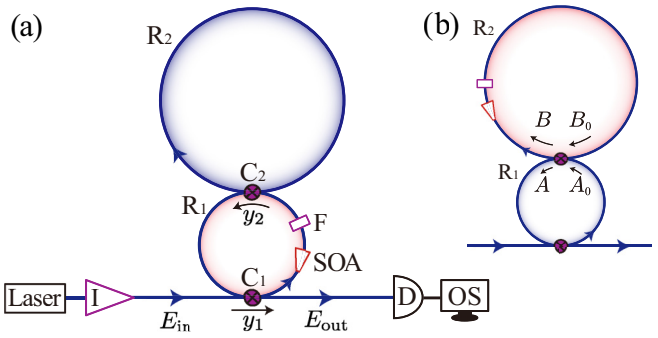

FIG. 1. (a) Schematic illustration of the experimental setup. R_1, R_2, first and second ring resonators; C_1 and C_2, couplers; SOA, InP/InGaAsP multiquantum well semiconductor optical amplifier; F, filter; I, isolator; D, detector; OS, oscilloscope; In and Out, input and output laser, respectively. The red (R_1) and blue (R_2) loops represent active (with gain) and passive (with loss) resonators, respectively. (b) Schematic illustration of the experimental setup for enhanced CRIT. A_0, A, B_0, and B are the positions at which the electric-field amplitudes are discussed.

the second resonator has gain. In this case, the system showed enhanced CRIT.

II. CRIT AND ATS

Figure 1 shows a schematic illustration of the experimental setup for the observation of the transition from inverted CRIT to ATS. Our system was similar to that used in previous experiments [24]. Briefly, the first (R_1) ring resonator and second (R_2) ring resonators were constructed using polarization-maintaining single-mode optical fibers. To implement gain, we placed an InP/InGaAsP multiquantum well semiconductor optical amplifier (SOA) in the first or the second ring resonator. SOA current control and attenuators were used to adjust the ring resonator loss or gain parameters. Coupling between R_1 and waveguide mode was achieved using a fixed ratio coupler (C_1). We controlled the coupling strength between R_1 and R_2 using a variable coupler (C_2). This coupler adjusted the intensity branching ratio between two bared fibers based on evanescent coupling. Although the branching ratio was calibrated independently, coupling hysteresis was observed. For this reason, we used the coupling strength as a parameter to fit the observed spectral structures. The raw data showing hysteresis of C_2 are given in the Supplemental Material [33]. An Er-fiber laser operating at 1556 nm served as the incident light source. The average power was 0.1 mW. The spectral width was 1 kHz, and the laser frequency was precisely tuned via piezoelectric control of the cavity length. The transmission spectra were recorded using an InGaP photodiode and a digital oscilloscope.

Directional coupling theory can be used to analyze the stationary input-output characteristics of coupled resonators [34].

$$\frac{E_{\text{out}}(\nu)}{E_{\text{in}}(\nu)} = (1-\gamma_1)^{1/2}\left\{\frac{y_1 - x_1 \text{Res}_2(\nu)\exp\left[i\phi_1(\nu)\right]}{1 - x_1 y_1 \text{Res}_2(\nu)\exp\left[i\phi_1(\nu)\right]}\right\} = \sqrt{T(\nu)}e^{i\theta(\nu)}, \tag{1}$$

where $E_{\text{in}}(\nu)$ and $E_{\text{out}}(\nu)$ represent input and output electric fields and

$$\text{Res}_2(\nu) = (1-\gamma_2)^{1/2}\left\{\frac{y_2 - x_2\exp\left[i(\phi_2(\nu)\right]}{1 - x_2 y_2 \exp\left[i\phi_2(\nu)\right]}\right\}.$$

The loss and gain parameter x_i represents the attenuation ($0 \leqslant x_i \leqslant 1$) or amplification ($1 \leqslant x_i$) of the electromagnetic field after one round trip in the ring resonator. The subscripts $i = 1, 2$ represent the first (R_1) and second (R_2) ring resonators, respectively. Parameter y_i ($0 \leqslant y_i \leqslant 1$) is the coupling parameter, which is the electric-field transmittance through the coupler. The coupling strength increases as y_1 decreases. Parameter γ_i represents the excess loss at the couplers, and $\phi_i(\nu)$ is the phase shift in the circulation orbit in ring resonator R_i. Equation (1) is an exposition of two distinct types of spectral lines, i.e., the spectral structures of CRIT and ATS, depending on the coupling parameter y_2. We developed an analysis technique that was applied to a normal EIT-ATS transition [30], in which gain was calculated by removing approximations and restrictions from parameters. We consider a situation $\phi_1(\nu) = \phi_2(\nu)$ in which both rings have equal cavity length. This condition is employed to simplify the analytical mathematical expression, but is not applicable to the experiments. In the experiments, Fano interference was examined at the resonance frequencies of both resonators. As the resonant linewidth depends on the cavity length, which is in turn determined by the free spectral range, the cavity length was considered during simulation. For simplicity, we ignored excess loss at the coupler and set $(1-\gamma_2)^{1/2} = 1$. Here, the approximation $\exp(i\phi) \approx 1 + i\phi$ is used, which is valid when $\phi \ll 1$; i.e., the resonance linewidth is narrow compared to the free spectral range. To extract the spectral resonance effects, we subtract the transmission electric field defined in Eq. (1) from the backgrund amplitude at the off-resonance frequency $E_{\text{back}}(\phi = \pi)$. Then, the transmission spectra can be separated into two Lorentz resonances [30]:

$$E_{\text{back}} - E(\phi) = E(\pi) - E(\phi) \approx \left\{\frac{A(y_2)}{\phi - Z_1(y_2)} + \frac{B(y_2)}{\phi - Z_2(y_2)}\right\}, \tag{2}$$

where $Z_1(y_2) = i\Gamma_c - \sqrt{\Lambda(y_2)}$ and $Z_2(y_2) = i\Gamma_c + \sqrt{\Lambda(y_2)}$ are poles of the two Lorentz-shaped resonances. The real and imaginary parts of $Z_1(y_2)$ and $Z_2(y_2)$ represent the resonance frequency and resonance linewidth for the transition, respectively. Γ_c and $\Lambda(y_2)$ are

$$\Gamma_c = \frac{-b}{2a}\Lambda = \frac{b^2 - 4ac}{(2a)^2},$$
$$a = -\frac{1}{2}(4x_1x_2y_1 - x_2y_2 - x_1y_1y_2) \times (1 + x_1x_2y_1 + x_2y_2 + x_1y_1y_2),$$
$$b = i(2x_1x_2y_1 - x_2y_2 - x_1y_1y_2) \times (1 + x_1x_2y_1 + x_2y_2 + x_1y_1y_2),$$
$$c = (1 + x_1x_2y_1)^2 - (x_2y_2 + x_1y_1y_2)^2.$$

$A(y_2)$ and $B(y_2)$ are the weights of the two functions.

$$A = \frac{eZ_1 + d}{Z_1 - Z_2} B = \frac{eZ_2 + d}{Z_2 - Z_1},$$
$$d = 2x_1 y_2 \left(1 - {x_2}^2\right)\left(1 - {y_1}^2\right),$$
$$e = -ix_1\left(1 - {y_1}^2\right)\left(2x_2 - y_2 + 3{x_2}^2 y_2\right).$$

We define a critical coupling parameter y_c as $\Lambda(y_c) = 0$. For the weak coupling condition, i.e., $y_c < y_2 < 1$, $\Lambda(y_2) < 0$, $Z_1(y_2)$, and $Z_2(y_2)$ are pure imaginary entities.

$$E_{\text{back}} - E(\phi) \propto \frac{A}{\phi - i\Gamma_{\text{narrow}}} + \frac{B}{\phi - i\Gamma_{\text{broad}}}, \tag{3}$$

where $\Gamma_{\text{narrow}} = \Gamma_c - \sqrt{-\Lambda(y_2)}$ and $\Gamma_{\text{broad}} = \Gamma_c + \sqrt{-\Lambda(y_2)}$. Then, the spectrum can be expressed as the sum of broad and narrow Lorentz functions with the same resonance frequency. This indicates that the system is in the CRIT regime. As the coupling strength increases when $0 < y_2 < y_c$, the discriminant becomes positive; i.e., $\Lambda(y_2) > 0$. Hence, Z_1 and Z_2 become complex values. The spectrum consists of two separated Lorentz line shapes at different resonance frequencies with the same spectral width:

$$E_{\text{back}} - E(\phi) \propto \frac{A}{\phi - (\Omega_{\text{low}} + i\Gamma_c)} + \frac{B}{\phi - (\Omega_{\text{high}} + i\Gamma_c)}, \tag{4}$$

where $\Omega_{\text{low}} = -\sqrt{\Lambda(y_2)}$ and $\Omega_{\text{high}} = \sqrt{\Lambda(y_2)}$. This indicates that the system is in the ATS regime.

Under the strong coupling condition, $y_2 < y_c$, the spectra showed an ATS double spectral structure. Whether the double structure appeared as doublet gain peaks or doublet absorption dips was dependent on the gain and loss parameters. The intensity difference between the on-resonance and off-resonance conditions in the ATS spectrum under the strong coupling limit is given as

$$\Delta I \equiv \left|E\left(y_2 = 0, \phi = \frac{\pi}{2}\right)\right|^2 - |E(y_2 = 0, \phi = 0)|^2$$
$$= \frac{-4x_1 x_2 y_1 [1 - (x_1 x_2)^2]\left(1 - {y_1}^2\right)}{[1 - (x_1 x_2 y_1)^2]^2}. \tag{5}$$

When $x_1 x_2 < 1$, $\Delta I < 0$, and the double dip structure appears in the ATS spectrum. This is reasonable because the total system is absorbing. However, when $x_1 x_2 > 1$, $\Delta I > 0$ and the double peak structure appeared in the ATS spectrum as the system became a gain system.

Figures 2(a) and 2(b) show the real and imaginary parts of $Z_1(y_2)$ and $Z_2(y_2)$, which represent the resonance frequency and resonance linewidth for the transition. The parameters used were those obtained experimentally, as shown in Fig. 3.

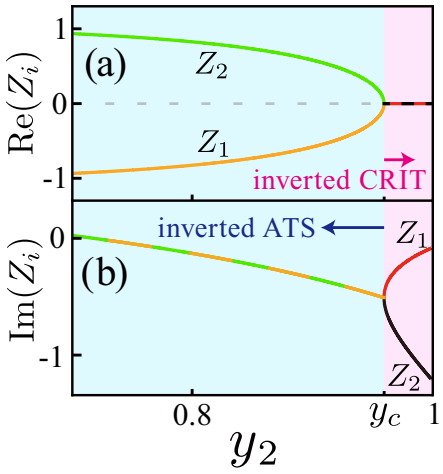

FIG. 2. (a), (b) Real and imaginary components, respectively, of Z_1 and Z_2 as a function of y_2 for the transition from inverted CRIT to inverted ATS. The parameters used were those obtained experimentally, as shown in Fig. 3. The critical coupling strength was $y_c = 0.96$. When $y_c < y_2 < 1$, the system is in the inverted CRIT regime (red), For $0 < y_2 < y_c$, the system is in the inverted ATS regime (blue).

III. EXPERIMENTS AND RESULTS

A. Transition from inverted CRIT to inverted ATS

We first examined the transition from inverted CRIT to inverted ATS as a function of the coupling strength between R_1 and R_2. For this experiment, R_1 had gain; hence, an SOA was placed in the first ring, R_1. The loss in R_2 was weak, to satisfy the condition $1 < x_1 x_2$, where x_1 and x_2 are the loss or gain parameters of R_1 and R_2, respectively. Column (a) of Fig. 3 shows the experimental results of the transmission spectra as a function of the laser detuning frequency, in which the coupling strength increased (coupling parameter y_2 decreased) from top to bottom. Figure 3(a1) shows the spectrum corresponding to when R_2 was decoupled; the spectrum showed a broad single peak relevant to the gain in R_1. Figure 3(a2) is the spectrum when R_2 was coupled. The second resonator R_2 induced a narrow dip (red upward arrow) in the broad gain peak due to R_1. As the coupling strength increased, this dip deepened. At the coupling strength shown in Fig. 3(a3), the transmission intensity level at the bottom of the dip was the same as the input intensity [blue dotted horizontal line in Fig. 3(a3)]. This dip was attributed to destructive interference between the two optical pathways: one path bypassed R_2, while the other passed through it. This is a demonstration of inverted CRIT, in which a nonamplifying window is induced in the frequency region where otherwise strong amplification would exist [30]. We examined the spectra in the stronger coupling region beyond the inverted CRIT region [Figs. 3(a4)–3(a7)]. As the coupling strength increased further, the dip deepened below the incident laser level and the bottom of the window reached the zero level [Fig. 3(a4)]. This is the critical coupling condition, in which the loss in the coupled system of R_1 and R_2 is balanced by the coupling of y_1. Except for a small reflection from the instrument, the light energy was totally absorbed in the ring resonator, which is reminiscent of a coherent perfect absorber [35]. As the coupling strength increased further, the spectrum split into two gain peaks at different frequencies with almost the same spectral width and intensity [orange and green downward arrows in Fig. 3(a6)]. We refer to this spectrum as inverted ATS ($y_2 < y_c$), in which the spectral structure is inverted (upside down) with respect to traditional/normal ATS splitting (normal ATS). Therefore, the

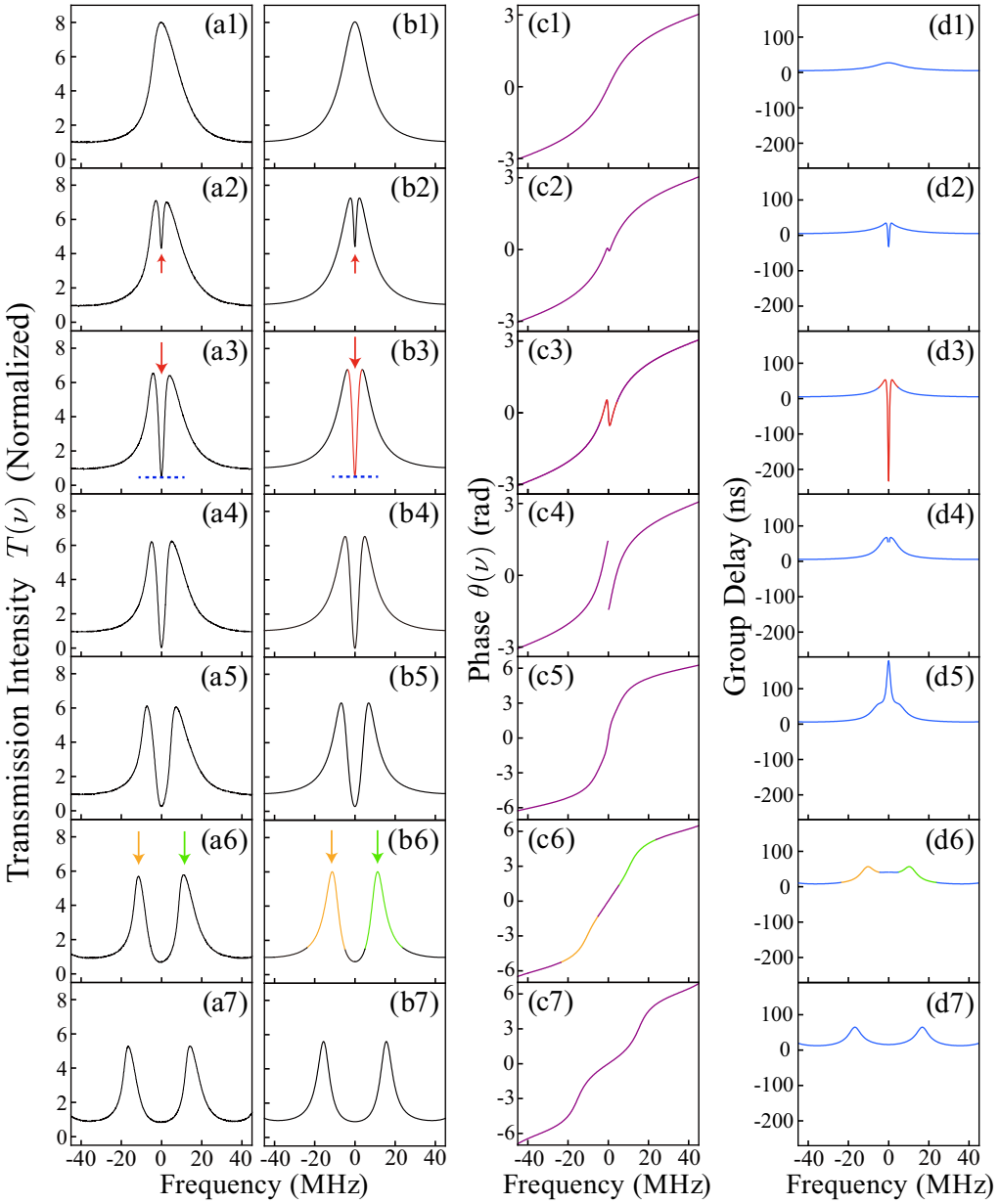

FIG. 3. Transition from inverted coupled-resonator-induced transparency (inverted CRIT) to an inverted Autler-Townes (inverted ATS) spectrum. (a) Experimental transmission spectra for inverted CRIT with different coupling strengths; the coupling strength increases from the top to the bottom. (b) The calculated curves of the transmission spectra shown in (a). Parameter y_2 is as follows: (b1) 1.0, (b2) 0.995, (b3) 0.98, (b4) 0.94, (b5) 0.87, (b6) 0.59, and (b7) 0.10. $x_1 = 1.9$, $x_2 = 0.92$, and $y_1 = 0.32$ in all figures. Resonator lengths were $L_1 = 3.1$ m, $L_2 = 5.3$ m. (c), (d) The transmission phase shift and group delay time, respectively, calculated using the same parameter obtained in (b). The colored parts in the calculated curves [the red parts in (b3), (c3), and (d3), and the orange and green parts in (b6), (c6), and (d6)] represent the same frequency regions. Animation of Fig. 3 with increased data points is given in the Supplemental Material [33].

experimental results shown in Figs. 3(a3)–3(a7) coincide with the steps in the transition from inverted CRIT to inverted ATS.

Column (b) in Fig. 3 shows the calculated curves for the transmission spectra to fit the experimental data shown in Fig. 3(a). We used the coupling strength y_2 as a parameter to accurately reproduce the observed spectral structures. For example, in Fig. 3(b2), the calibrated value of y_2 of the coupler C_2 was in the range $0.995 < y_2 < 0.998$ owing to the hysteresis, while the value used in the fitting was $y_2 = 0.995$, so the two values showed a reasonable agreement. All other parameters, x_1, x_2, and y_1, were assigned fixed values that were determined by independent measurement. Using the parameters obtained in Fig. 3(b) and Eq. (2), we calculated the critical value as $y_c = 0.96$ for the transition from inverted CRIT to inverted ATS. This value of y_c lies between Figs. 3(b3) and 3(b4) and reasonably distinguishes the spectral structures shown in Fig. 3.

The unique features of the spectra and dispersion in traditional CRIT have allowed for the development of many applications. For example, the lossless, steep, and controllable

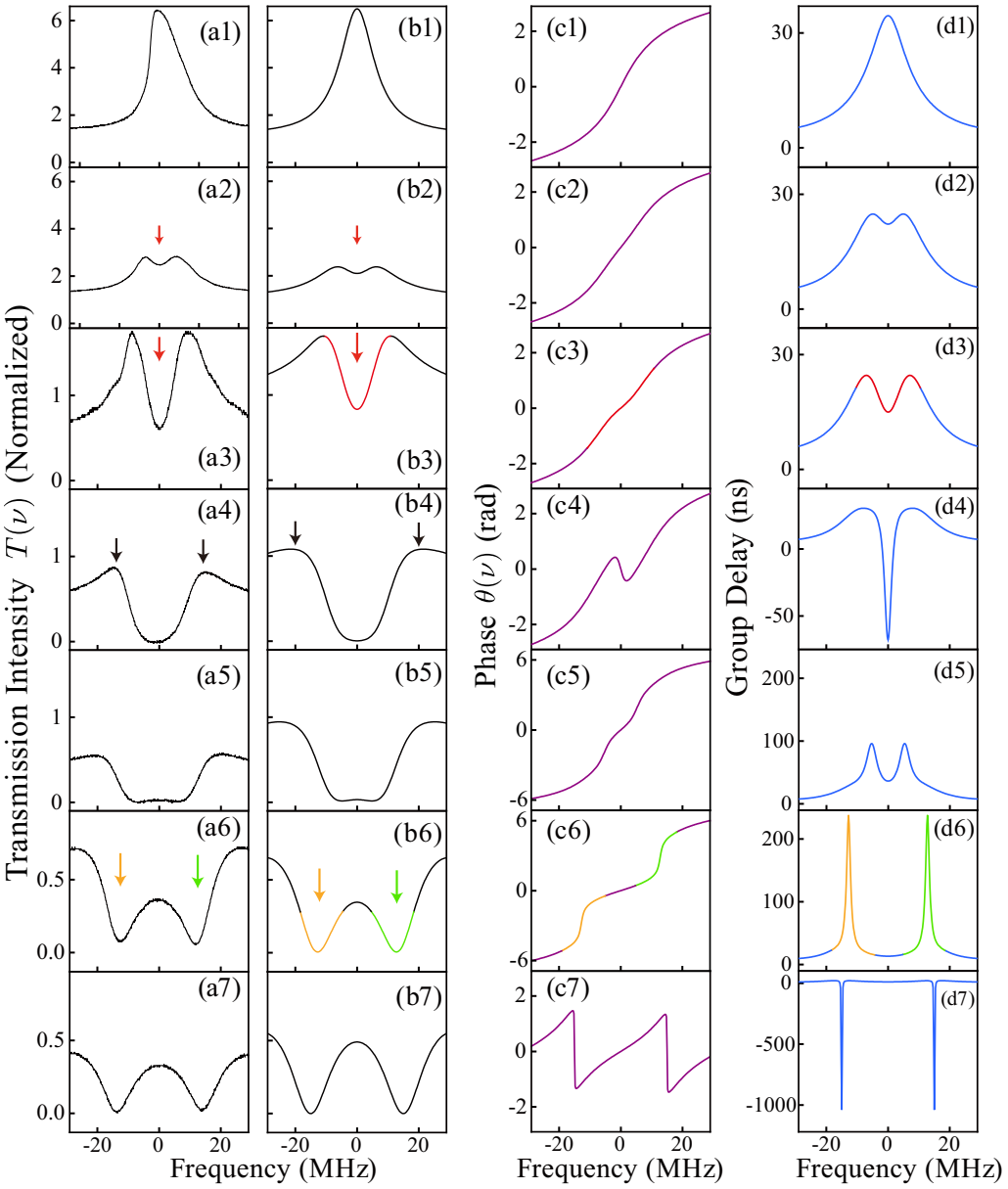

FIG. 4. Transition from inverted CRIT to normal ATS. (a) Experimental observation of transmission spectra for inverted CRIT spectra for the different coupling strengths; the coupling strength increases from top to bottom. (b) Calculated curves of the transmission spectra shown in (a). Parameter y_2 is as follows: (b1) 1.0, (b2) 0.90, (b3) 0.82, (b4) 0.59, (b5) 0.48, (b6) 0.17, and (b7) 0.04. $x_1 = 1.4$, $x_2 = 0.3$, and $y_1 = 0.45$ in all figures. (c), (d) Transmission phase shift and group delay time, respectively, calculated using the same parameter obtained in (b). The colored parts in the calculated curves [red parts in (b3), (c3), and (d3) and the orange and green parts in (b6), (c6), and (d6)] represent the same frequency regions.

dispersion in the transparency window in normal CRIT realizes slow light and frozen light [15]. In contrast to the normal dispersion in normal CRIT, anomalous dispersion appears in inverted CRIT. Figures 3(c) and 3(d) show the transmission phase shift and the group delay, respectively, calculated using the same parameters obtained in the fitting in Fig. 3(b). When R_2 was decoupled, the transmission phase shift increased monotonically as a function of the detuning frequency [Fig. 3(c1)]; hence, the group delay was positive and slow light was expected [Fig. 3(d1)]. When the R_2 was coupled and the induced window appeared [red arrows in Figs. 3(b2) and 3(b3)], the transmission phase shift in the window showed anomalous dispersion [Fig. 3(d2)]. For the given coupling strength shown in Fig. 3(b3), with the condition that the transmittance was 1, the incident pulse propagated with superluminal group velocity without amplification or attenuation [24,25]. Under critical coupling conditions, where the bottom of the induced window reached a zero level, the transmission phase reached $\pi/2$ [Fig. 3(c4)]. As the coupling strength increased further, the spectrum showed an inverted-ATS-type spectrum, and the two gain peaks displayed normal dispersion [Figs. 3(c7) and 3(d7)].

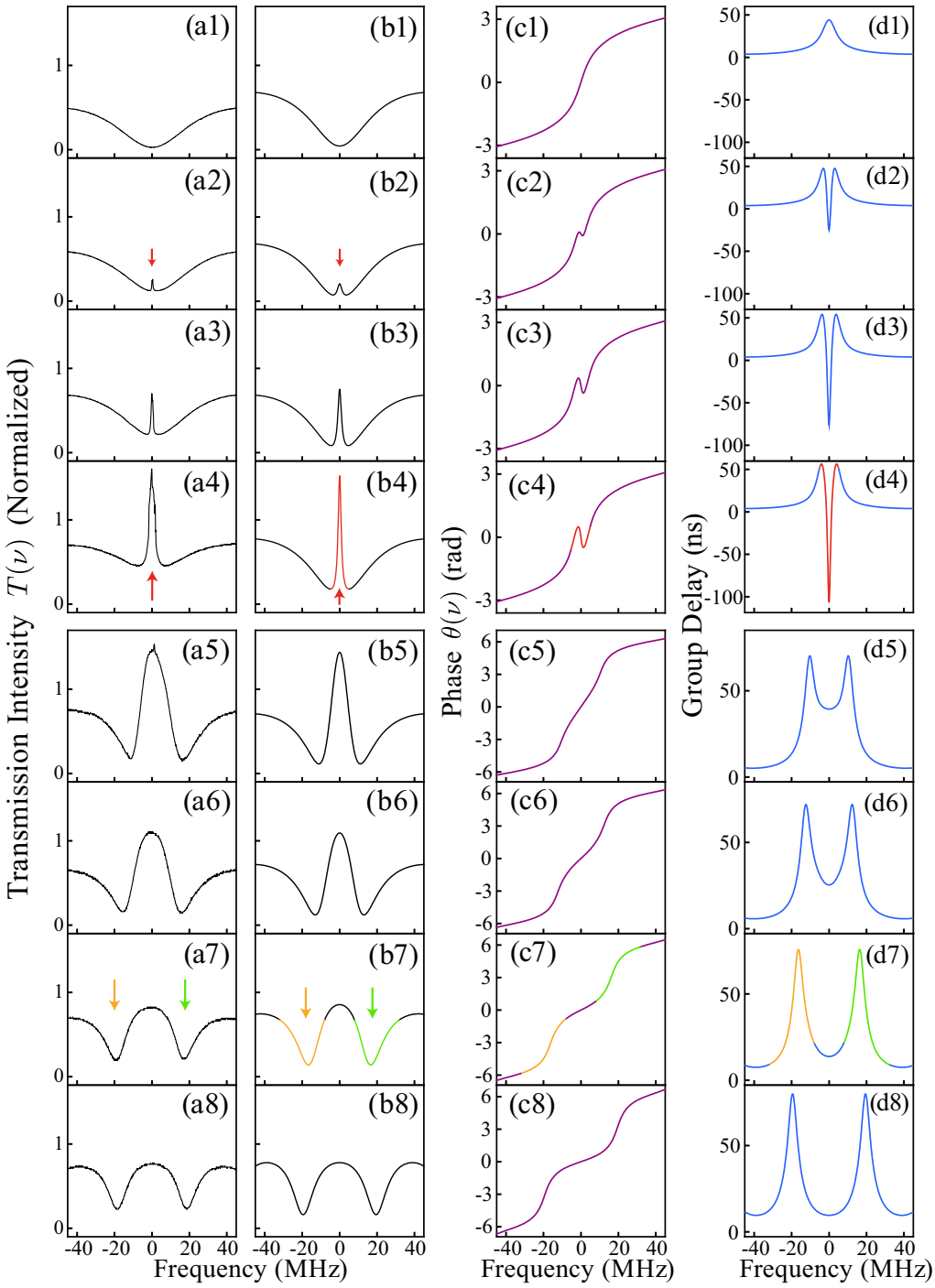

FIG. 5. Transition from enhanced CRIT to normal ATS. (a) Experimental observation of transmission spectra for the enhanced CRIT spectra for the different coupling strengths. The coupling strength increased from top to bottom. (b) The calculated curves of the transmission spectra shown in (a). Parameter y_2 is as follows: (b1) 1.0, (b2) 0.98, (b3) 0.96, (b4) 0.95, (b5) 0.67, (b6) 0.54, (b7) 0.25, and (b8) 0.00. $x_1 = 0.60$, $x_2 = 1.2$, and $y_1 = 0.45$ in all figures. (c), (d) Transmission phase shift and group delay time, respectively, calculated using the same parameter obtained in (b). The colored parts in calculated curves [red parts in (b4), (c4), and (d4) and the orange and green parts in (b7), (c7), and (d7)] represent the same frequency regions.

B. Transition from inverted CRIT to normal ATS

In contrast to Fig. 3, when the loss in R_2 was large as $1 > x_1x_2$, a different type of transition appeared. For this experiment, an additional attenuator was implemented in R_2. Figure 4(a) shows the experimental results for the transmission spectra, for the different coupling strengths. A similar discussion to that for Fig. 3 is applicable. When R_2 was coupled, an induced window was observed [red downward arrow in Fig. 4(a2)]. In comparison with Fig. 3(a2), the width of the induced window was broad. This occurred because the loss in

R_2 was large. As the coupling strength increased, the dip in the spectrum deepened [Fig. 4(a3)], as in the case of a small loss [Fig. 3(a3)]. Simultaneously, however, the height of the gain shoulders below and above the resonance frequency was reduced [black downward arrow in Fig. 4(a4)]. This occurred because the large loss in R_2 was mixed into R_1, and the total loss of the coupled system of R_1 and R_2 increased. As the coupling strength increased further, the dip deepened and the bottom reached a zero level [Fig. 4(a4)]; thus, the critical coupling condition was achieved. As the coupling strength continued to increase, the resonances appeared as dips in the transmission spectrum of Fig. 4(a7). These dips are in contrast to the gain peaks observed in Fig. 3(a7). As $1 > x_1x_2$, the loss in R_2 overcame the gain in R_1; therefore, the coupled system was an absorbing system as a whole. The experimental results shown in Figs. 4(a3)–4(a7) show the transition from inverted CRIT to typical ATS. Column (b) of Fig. 4 shows the calculated curves of the transmission spectra, which showed good agreement with the experimental observation shown in column (a). A phase map similar to Fig. 2 was obtained from the experimental parameters used for fitting, as shown in Fig. 4, and the critical coupling strength was calculated as $y_c = 0.72$. This value of y_c lies between Figs. 4(b3) and 4(b4). For this transition, the spectra transformed via complex structures; thus the discrimination between CRIT and ATS was not clear from the observed spectral changes. The critical coupling strength calculated above, however, could uniquely separate the CRIT and ATS regimes.

Figures 4(c), and 4(d) show phase shift and group delay, respectively, calculated using the same parameters obtained in the fitting shown in Fig. 4(b). The dispersion relation jumped from normal to anomalous dispersion when the coupling strength crossed the critical coupling condition [Figs. 4(c6)–4(c7)]. In contrast to Fig. 3(c7), the two absorption dips in the normal ATS spectrum indicate anomalous dispersion [Fig. 4(c7)].

C. Enhanced CRIT

So far, we have discussed the Fano interference effect in cases in which R_1 had gain and R_2 was an absorbing resonator. Next, we discuss the case in which R_2 has gain. For this experiment, the SOA was removed from R_1 and implemented in R_2. Figure 5(a) shows the experimental observation of the transmission spectra for different coupling strengths. Figure 5(a1) displays the transmission spectra when R_2 was decoupled. The transmission spectra showed a broad dip due to the absorption in R_1. Figures 5(a2)–5(a7) show the transmission spectra when R_2 was coupled to R_1; in the figure, the coupling strengths increase from top to bottom. The spectrum shown in Fig. 5(a2) was acquired when R_2 was weakly coupled to R_1. Within the broad dip due to the absorbing R_1, a small and narrow peak appeared. As the coupling strength of R_2 increased, the height of this peak increased [Figs. 5(a3)–5(a4)]. In contrast to traditional CRIT, this peak increased strongly beyond the intensity level of the incident light.

Although the spectra from Figs. 5(a1)–5(a8) seemed to transform continuously, there were significant differences in the system operation. We classified the operation into three regimes. Regimes I and III correspond to the spectra between Figs. 5(a2)–5(a4) and 5(a5)–5(a8), respectively, with regime II in between. The experimental spectra of regimes I and III were stable; however, that of regime II showed instability. In regime II, the output intensity jumped to high levels (not shown in Fig. 5). We consider that this jump in the output intensity was attributable to lasing action within R_2. Figure 1(b) is a schematic illustration of the coupled ring resonator for enhanced CRIT. We introduced electric fields $E_{A_0} = 1$, E_A, E_{B_0}, and E_B at points A_0, A, B_0, and B, respectively. Using Eq. (1), the electric field in R_2 is represented as $E_B = -\frac{i\sqrt{1-y_2^2}e^{i\phi}}{1-x_2y_2e^{i\phi}}$. At $x_2y_2 = 1$, laser action was expected under the condition $\phi = 0$. Regime I is notable from the perspective that the system was stable even though $x_2y_2 > 1$. After one round trip in R_2, the electric-field amplitude at B_0 increased by an amount $\Delta E_{B_0} = |y_2x_2E_{B_0}| - |E_{B_0}| > 0$. This increment was canceled by the π radian-shifted electric field coupled from E_{A_0}. The field intensity in R_2 was steady, even under the condition $x_2y_2 > 1$. Figure 5(a4) shows that the intensity of the induced window (peak) was much higher than the incident laser level. We refer to this spectrum structure as enhanced CRIT. Figures 5(a5)–5(a8) show the spectra observed when the coupling further increased and the condition $x_2y_2 < 1$ was satisfied (regime III). After one round trip in R_2, the electric-field amplitude decreased by an amount $\Delta E_{B_0} = |y_2x_2E_{B_0}| - |E_{B_0}| < 0$. This decrease was compensated by the addition of the phase-matched electric field supplied from E_{A_0} via the coupler. As the coupling strength further increased, the spectral width of the peak broadened, and the peak height decreased further. Finally, the spectrum transformed into the normal ATS spectra [Fig. 5(a8)]. This occurred as the total loss of the system satisfied the condition $x_1x_2 < 1$; hence, the coupled resonator as a whole is an absorbing system. Column (b) of Fig. 5 shows the calculated curves of the transmission spectra, which showed good agreement with the experimental observation shown in column (a). Columns (c) and (d) show the transmission phase shift and the group delay time, respectively, calculated using the same parameters as those for column (b) in the same row. Under the condition $x_2y_2 > 1$, the transmission phase showed anomalous dispersion [Figs. 5(c2)–5(c4)]. Using the experimental parameters

TABLE I. The three types of transition from CRIT to ATS are shown in Figs. 3–5. Conditions x_1 and x_2 are summarized.

	Transition		
Parameter	Inverted CRIT → inverted ATS (Fig. 3)	Inverted CRIT → normal ATS (Fig. 4)	Enhanced CRIT → normal ATS (Fig. 5)
x_1	1.92 (>1)	1.40 (>1)	0.60 (<1)
x_2	0.92 (<1)	0.30 (<1)	1.20 (>1)
x_1x_2	1.77 (>1)	0.42 (<1)	0.72 (<1)

shown in Fig. 5 and Eq. (2), we calculated the critical value $y_c = 0.70$ for the transition from enhanced CRIT to normal ATS, as shown in Fig. 5. This value of y_c lies between Figs. 5(b4) and 5(b5).

The three types of transition from CRIT to ATS discussed in Figs. 3–5 are summarized in Table I.

IV. SUMMARY

We systematically examined the transition from inverted and enhanced CRIT to ATS. As the coupling strength between two resonators increased, the inverted CRIT spectrum transitioned into inverted or normal ATS, respectively, depending on the loss parameter. The spectra were transformed via complex structures, so CRIT and ATS could not be clearly discriminated based on the observed spectral changes. The critical coupling strength y_c was calculated using a model that separated the response function into double Lorentz line shapes, and could uniquely separate the CRIT and ATS regimes. When the second resonator had gain, the system showed enhanced CRIT, in which the intensity of the induced window (peak) was much higher than the incident laser level. The diversity in the spectral structures and dispersions in inverted and enhanced CRIT and ATS offer flexibility in photonic designs. Furthermore, when active optical resonators are coupled to other freedoms, such as mechanical or plasmon freedom, inverted optomechanical-induced transparency or inverted plasmon-induced transparency, as well as ATS, could be realized; they have potential in practical applications.

[1] U. Fano, Effects of configuration interaction on intensities and phase shifts, Phys. Rev. **124**, 1866 (1961).

[2] M. F. Limonov, M. V. Rybin, A. N. Poddubny, and Y. S. Kivshar, Fano resonances in photonics, Nat. Photonics **11**, 543 (2017).

[3] K.-J. Boller, A. Imamoğlu, and S. E. Harris, Observation of Electromagnetically Induced Transparency, Phys. Rev. Lett. **66**, 2593 (1991).

[4] S. E. Harris, Electromagnetically induced transparency, Phys. Today **50**(7), 36 (1997).

[5] D. D. Smith, H. Chang, K. A. Fuller, A. T. Rosenberger, and R. W. Boyd, Coupled-resonator-induced transparency, Phys. Rev. A **69**, 063804 (2004).

[6] A. Naweed, G. Farca, S. I. Shopova, and A. T.Rosenberger, Induced transparency and absorption in coupled whispering-gallery microresonators, Phys. Rev. A **71**, 043804 (2005).

[7] Q. Xu, S. Sandhu, M. L. Povinelli, J. Shakya, S. Fan, and M. Lipson, Experimental Realization of an On-Chip All-Optical Analogue to Electromagnetically Induced Transparency, Phys. Rev. Lett. **96**, 123901 (2006).

[8] K. Totsuka, N. Kobayashi, and M. Tomita, Slow Light in Coupled-Resonator-Induced Transparency, Phys. Rev. Lett. **98**, 213904 (2007).

[9] S. T. Guo, Y. H. Zhang, L. L. Wu, M. Y. Ye, and X. M. Lin, Transition between coupled-resonator-induced transparency and absorption, Phys. Rev. A **103**, 033510 (2021).

[10] S. Zhang, D. A. Genov, Y. Wang, M. Liu, and X. Zhang, Plasmon-Induced Transparency in Metamaterials, Phys. Rev. Lett. **101**, 047401 (2008).

[11] N. Papasimakis, V. A. Fedotov, N. I. Zheludev, and S. L. Prosvirnin, Metamaterial Analog of Electromagnetically Induced Transparency, Phys. Rev. Lett. **101**, 253903 (2008).

[12] N. Liu, L. Langguth, T. Weiss, J. Kästel, M. Fleischhauer, T. Pfau, and H. Giessen, Plasmonic analogue of electromagnetically induced transparency at the Drude damping limit, Nat. Mater. **8**, 758 (2009).

[13] S. Weis, R. Rivière, S. Deléglise, E. Gavartin, O. Arcizet, A. Schliesser and T. J. Kippenberg, Optomechanically induced transparency, Science **330**, 1520 (2010).

[14] Q. Lin, J. Rosenberg, D. Chang, R. Camacho, M. Eichenfield, K. J. Vahala, and O. Painter, Coherent mixing of mechanical excitations in nano-optomechanical structures, Nat. Photonics **4**, 236 (2010).

[15] J. B. Khurgin and R. S. Tucker, *Slow Light: Science and Applications* (CRC Press, Boca Raton, FL, 2008).

[16] W. Yoshiki, Y. Honda, T. Tetsumoto, K. Furusawa, N. Sekine, and T. Tanabe, All-optical tunable buffering with coupled ultra-high Q whispering gallery mode microcavities, Sci. Rep. **7**, 10688 (2017).

[17] M. Heuck, P. T. Kristensen, Y. Elesin, and J. Mørk, Improved switching using Fano resonances in photonic crystal structures, Opt. Lett. **38**, 2466 (2013).

[18] J. Liao, X. Wu, L. Liu, and L. Xu, Fano resonance and improved sensing performance in a spectral-simplified optofluidic microbubble resonator by introducing selective modal losses, Opt. Express **24**, 8574 (2016).

[19] C.-Y. Chao and L. J. Guo, Biochemical sensors based on polymer microrings with sharp asymmetrical resonance, Appl. Phys. Lett. **83**, 1527 (2003).

[20] Y. Yu, A. Sakanas, A. R. Zali *et al.*, Ultra-coherent Fano laser based on a bound state in the continuum, Nat. Photonics **15**, 758 (2021).

[21] Y. Dumeige, Thi Kim Ngân Nguyên, L. Ghişa, S. Trebaol, and P. Féron, Measurement of the dispersion induced by a slow-light system based on coupled active-resonator-induced transparency, Phys. Rev. A **78**, 013818 (2008).

[22] M. Asano, Ş. K. Özdemir, W. Chen, R. Ikuta, L. Yang, N. Imoto, and T. Yamamoto, Controlling slow and fast light and dynamic pulse-splitting with tunable optical gain in a whispering-gallery-mode microcavity, Appl. Phys. Lett. **108**, 181105 (2016).

[23] S. Trebaol, T. K. N. Nguyên, H. Tavernier, L. Ghişa, Y. Dumeige, and P. Féron, Artificial dispersion of active optical coupled resonator systems, C. R. Phys. **10**, 964 (2009).

[24] T. Oishi and M. Tomita, Inverted coupled-resonator-induced transparency, Phys. Rev. A **88**, 013813 (2013).

[25] D. Sugio, K. Yoshimura, K. Nakamura, T. Manabe, and M. Tomita, Propagation of a peak-truncated Gaussian pulse in an inverted coupled-resonator-induced transparency system, Opt. Commun. **520**, 128466 (2022).

[26] H. Jing, S. K. Özdemir, Z. Geng, J. Zhang, X-Y. Lü, B. Peng, L. Yang, and F. Nori, Optomechanically-induced transparency in parity-time-symmetric microresonators, Sci. Rep. **5**, 9663 (2015).

[27] T. Y. Abi-Salloum, Electromagnetically induced transparency and Autler-Townes splitting: Two similar but distinct phenom-

ena in two categories of three-level atomic systems, Phys. Rev. A **81**, 053836 (2010).

[28] P. M. Anisimov, J. P. Dowling, and B. C. Sanders, Objectively Discerning Autler-Townes Splitting from Electromagnetically Induced Transparency, Phys. Rev. Lett. **107**, 163604 (2011).

[29] L. Giner, L. Veissier, B. Sparkes, A. S. Sheremet, A. Nicolas, O. S. Mishina, M. Scherman, S. Burks, I. Shomroni, D. V. Kupriyanov, P. K. Lam, E. Giacobino, and J. Laurat, Experimental investigation of the transition between Autler-Townes splitting and electromagnetically-induced-transparency models, Phys. Rev. A **87**, 013823 (2013).

[30] T. Oishi, R. Suzuki, A. I. Talukder, and M. Tomita, Transition from an optical precursor in coupled-resonator-induced transparency to coherent energy exchange in Autler-Townes splitting, Phys. Rev. A **88**, 023847 (2013).

[31] B. Peng, Ş. K. Özdemir, W. Chen, F. Nori, and L. Yang, What is and what is not electromagnetically induced transparency in whispering-gallery microcavities, Nat. Commun. **5**, 5082 (2014).

[32] H. Wu, Y. Ruan, Z. Li, M.-X. Dong, M. Cai, J. Tang, L. Tang, H. Zhang, M. Xiao, and K. Xia, Fundamental distinction of electromagnetically induced transparency and Autler–Townes splitting in breaking the time-reversal symmetry, Laser Photonics Rev. **16**, 2100708 (2022).

[33] See Supplemental Material at http://link.aps.org/supplemental/10.1103/PhysRevA.107.013110 for the raw data showing hysteresis of C_2 and animation of Fig. 3 with increased data points.

[34] K. Totsuka and M. Tomita, Slow and fast light in a microsphere-optical fiber system, J. Opt. Soc. Am. B **23**, 2194 (2006).

[35] Y. D. Chong, L. Ge, H. Cao, and A. D. Stone, Coherent Perfect Absorbers: Time-Reversed Lasers, Phys. Rev. Lett. **105**, 053901 (2010).